RESEARCH ARTICLE

Correspondence to:
M. F. Thomsen,
mthomsen@psi.edu

Ion composition in interchange injection events in Saturn's magnetosphere

M. F. Thomsen[1], D. B. Reisenfeld[2], R. J. Wilson[3], M. Andriopoulou[4], F. J. Crary[3], G. B. Hospodarsky[5], C. M. Jackman[6], X. Jia[7], K. K. Khurana[8], C. Paranicas[9], E. Roussos[10], N. Sergis[11], and R. L. Tokar[1]

[1]Planetary Science Institute, Tucson, Arizona, USA, [2]Department of Physics and Astronomy, University of Montana, Missoula, Montana, USA, [3]Laboratory for Atmospheric and Space Physics, University of Colorado, Boulder, Colorado, USA, [4]Austrian Academy of Sciences, Graz, Austria, [5]Department of Physics and Astronomy, University of Iowa, Iowa City, Iowa, USA, [6]Department of Physics and Astronomy, University of Southampton, Southampton, UK, [7]Department of Atmospheric, Oceanic, and Space Sciences, University of Michigan, Ann Arbor, Michigan, USA, [8]Institute of Geophysics and Planetary Physics, University of California, Los Angeles, California, USA, [9]Applied Physics Laboratory, Johns Hopkins University, Laurel, Maryland, USA, [10]Max Planck Institute for Solar System Research, Göttingen, Germany, [11]Academy of Athens, Athens, Greece

Abstract Interchange injection events are commonly observed by the Cassini spacecraft in the region between about 6 and 12 R_s (1 R_s = 60,268 km) and even frequently beyond. In this study, 13 examples of interchange injection events are identified in Cassini/Cassini Plasma Spectrometer data under special conditions such that time-of-flight (TOF) mass spectra could be obtained from entirely within the events. Using the TOF data to separate the main ion species H^+, H_2^+, and W^+, approximate densities of each species are calculated under the assumption that all distributions were isotropic. The light-ion density ratios, H_2^+/H^+, in the injection events are not discernibly different from those ratios in control intervals from the ambient plasma. However, the water-group ratio, W^+/H^+, is significantly lower than ambient. The comparison of the measured density ratios with the range of values observed throughout Saturn's magnetosphere indicates that the values of W^+/H^+ that are as low as those observed within the injection events are found primarily beyond L~14 (where L is the equatorial crossing distance, in Saturn radius, of a dipole field line), indicating that the injection events are delivering plasma from the outer magnetosphere at times traveling at least 6 R_s.

1. Introduction

Saturn's magnetospheric dynamics are to a large extent determined by two important factors: (1) The dominant source of magnetospheric plasma is the ionization of water molecules released by the moon Enceladus deep within the magnetosphere, and (2) the magnetosphere is strongly coupled to the ionosphere and nearly corotates with the planet at a rapid rate. As a consequence of the internal plasma source and the rapid rotation, plasma is transported from the near-planet source region out through the outer magnetosphere for ultimate loss to the solar wind.

A number of studies have now demonstrated observationally [e.g., *Burch et al.*, 2005; *Hill et al.*, 2005; *Mauk et al.*, 2005; *André et al.*, 2005, 2007; *Rymer et al.*, 2009] and theoretically [e.g., *Kidder et al.*, 2009; *Liu et al.*, 2010; *Liu and Hill*, 2012] that the main transport process moving plasma from the inner to the outer magnetosphere (~5–12 R_s) is an interchange instability driven by the strong centrifugal forcing by rapid magnetospheric rotation (for a brief review, see *Thomsen* [2013]). In this process, relatively cool and dense plasma produced in the inner magnetosphere is driven outward, while hotter, less dense plasma from the outer magnetosphere takes its place. The result is the penetration of flux tubes or fingers of outer magnetospheric plasma deep into the inner magnetosphere. These structures, known as interchange injections, are seen very commonly by the Cassini spacecraft during its traversals of Saturn's inner magnetosphere.

While much has been done to characterize the properties of interchange injections, and there has been considerable success in numerical modeling of the instability, there remain important questions about their initiation, structure, and evolution. For example, we still do not know exactly where the instability is initiated and whether it is spontaneous or in some sense driven by other magnetospheric processes such as tail reconnection.

Table 1. TOF Accumulation Times

CAPS Telemetry Rate	TOF Accumulation Time
500 bits/s	No TOF returned
1 kbits/s	512 s
2 kbits/s	512 s
4 kbits/s	256 s
8 kbits/s	256 s
16 kbits/s	256 s

One clue to help answer these questions is the nature of the injected plasma itself, which should have properties characteristic of the outer magnetosphere where the inflow began. *Rymer et al.* [2009] looked at the adiabatic mapping of the injected hot electron population to estimate that the origin of six interchange events observed at $L\sim7$–8 was beyond 8–9 R_s. They further mapped the observed pitch angle distributions to infer that the source location was probably between ~10 and 12 R_s.

Other plasma properties of interchange injections are also potentially useful for inferring the location where the inflow was initiated. However, most of these properties (such as the plasma density and temperature) are affected by the transport, and assumptions regarding the adiabaticity are necessary to enable a mapping to the source region (as done, for example, by *Rymer et al.* [2008, 2009]). By contrast, the ion composition of the injected plasma should not change as the material is transported inward as long as the transport is rapid enough that there is not significant mixing with the inner magnetospheric plasma as the injection occurs. This should be the case for relatively "young" injections, i.e., those for which there is very little drift dispersion apparent at the higher energies, as well as an absence of lower energy plasma characteristic of the inner magnetosphere [e.g., *Burch et al.*, 2005].

The magnetospheric ion composition is known to vary with radial distance from Saturn [e.g., *Thomsen et al.*, 2010], although the exact reason for this is not well established. It may be due to the admixture of light ions originating in Titan's neutral atom torus, or it may be a consequence of preferential loss of heavy ions in magnetotail reconnection [e.g., *Badman and Cowley*, 2007; *Thomsen et al.*, 2013]. In any event, the observed variation of ion composition with radial distance offers the opportunity to establish the distance from which the observed injected plasma began its inward motion.

In this paper we use ion composition measurements from the Cassini Plasma Spectrometer (CAPS) to characterize the H_2^+/H^+ and W^+/H^+ ratios within a number of identified interchange injection events at Saturn (here "W^+" refers to water-group ions, i.e., O^+, OH^+, H_2O^+, and H_3O^+). We compare the ion composition within the events to the composition within "control" intervals of ambient inner magnetospheric plasma observed near the injections. We also compare the composition within the events with a statistical characterization of the composition observed by CAPS throughout the inner and outer magnetosphere.

2. Data

The Cassini Plasma Spectrometer (CAPS) consists of three separate analyzers: an electron spectrometer (ELS), an ion beam spectrometer (IBS), and a hot ion mass spectrometer (IMS) [*Young et al.*, 2004]. The IMS is a top-hat electrostatic analyzer to provide ion E/q (energy per charge) information, followed by a novel linear electric field time-of-flight (TOF) section to provide ion mass information. The IMS produces several data products with different cadences depending on the instrument telemetry rate.

The so-called singles (SNG) data correspond to the start signals in the TOF section, so they indicate only the energy per charge of the ions and not their species. However, SNG data have sufficient angular information to derive the plasma moments (density, flow velocity, and temperature) of the ion distribution [e.g., *Thomsen et al.*, 2010; *Wilson et al.*, 2008]. In order to partition the non-mass-identified SNG counts into the appropriate species for calculation of moments, the analysis of *Wilson et al.* [2008] relies on the separation by energy of light and heavy species flowing at the same speed, with the requirement that the temperatures be sufficiently cool to prevent much overlap in the peaks. For the hot populations in injection events, this condition is not met, and the two main species cannot be distinguished. Likewise, the computation of numerical moments from SNG data [e.g., *Thomsen et al.*, 2010] partitions SNG counts into different species based on nearly concurrent TOF measurements, routinely using several TOF spectra (see below) to determine the partition. This partition is strongly time aliased for brief events such as interchange injections, so numerical SNG moments are not reliable for our purposes, and we need to use the TOF data themselves.

Table 2. Intervals Suitable for Composition Determination

Date	Start	End	Δt (min)	Maglat (deg)	R (R_s)	Start Bcycle	End Bcycle	1 = inj; 2 = control	nH (cm^{-3})	nH$_2$ (cm^{-3})	nW (cm^{-3})	nH$_2$/nH	nW/nH
27/5/2007	13:25:30	13:34:01	8.52	−14.9	8.89	189	190	1	0.00829	0.00125	0.00327	0.151	0.394
27/5/2007	13:38:18	13:42:33	4.25	−14.8	8.97	192	192	1	0.0141	0.00220	0.00630	0.156	0.447
27/5/2007	14:38:02	15:03:37	25.58	−13.5	9.52	206	207	1	0.00640	0.00142	0.00373	0.222	0.583
27/5/2007	12:40:00	12:50:00	10.00	−15.8	8.53			2	0.152	0.0160	0.131	0.105	0.862
27/5/2007	14:00:00	14:10:00	10.00	−14.3	9.16			2	0.157	0.0130	0.194	0.0828	1.24
24/10/2007	19:26:13	19:34:44	8.52	−3.5	8.24	274	275	1	0.00961	0.00192	0.00774	0.200	0.805
24/10/2007	19:47:33	20:00:20	12.78	−3.4	8.38	279	281	1	0.00715	0.00138	0.00709	0.193	0.992
24/10/2007	20:20:00	20:30:00	10.00	−3.3	8.67			2	0.110	0.0220	0.858	0.200	7.80
18/11/2007	3:47:18	3:55:49	8.52	−2.0	12.03	54	55	1	0.00717	0.00174	0.00569	0.243	0.794
18/11/2007	3:20:00	3:30:00	10.00	−2.1	11.84			2	0.0372	0.0131	0.241	0.352	6.48
12/2/2010	23:01:37	23:14:24	12.78	0.2	11.31	160	162	1	0.0205	0.00470	0.00800	0.229	0.390
12/2/2010	22:30:00	22:50:00	20.00	0.2	11.51			2	0.0553	0.0187	0.135	0.338	2.44
2/3/2010	16:02:14	16:10:45	8.52	0.3	9.53	154	155	1	0.0553	0.0132	0.0889	0.239	1.61
2/3/2010	16:20:00	16:40:00	20.00	0.3	9.33			2	0.325	0.0880	1.001	0.271	3.08
27/4/2010	5:25:56	5:34:27	8.52	−0.0	10.38	77	78	1	0.0209	0.00950	0.0326	0.455	1.56
27/4/2010	5:00:00	5:20:00	20.00	−0.0	10.53			2	0.0677	0.0277	0.754	0.409	11.1
19/5/2010	9:18:14	9:48:05	29.85	0.1	14.08	131	137	1	0.00366	0.00133	0.00259	0.363	0.708
19/5/2010	9:52:22	10:13:41	21.32	0.1	14.28	139	143	1	0.00418	0.00161	0.00777	0.385	1.86
19/5/2010	10:43:34	11:00:37	17.05	0.1	14.59	151	154	1	0.00557	0.00221	0.00409	0.397	0.734
19/5/2010	8:50:00	9:10:00	20.00	0.1	13.87			2	0.0490	0.0209	0.211	0.426	4.31
2/6/2010	12:17:17	12:30:04	12.78	11.6	12.01	173	175	1	0.0160	0.00461	0.0151	0.288	0.944
2/6/2010	11:50:00	12:10:00	20.00	11.6	12.18			2	0.0881	0.0195	0.136	0.221	1.54

Because of the lower efficiency for full time-of-flight determinations, the mass-resolved (TOF) data are summed onboard over all look directions (all eight IMS detectors and all actuation angles) over an accumulation interval that is either 512 s or 256 s, depending on the telemetry (see Table 1). This interval is termed a "Bcycle" of data. These data are returned as the TOF data product, which is a matrix of 32 energy channels (ranging from ~1 eV to ~33 keV) by 256 time-of-flight channels. The mapping of this matrix to ion species is discussed in the Appendix A. (Note that in this paper we also refer to energy channels as "energy levels.")

In addition to the intrinsically long accumulation times required to obtain a TOF spectrum, overall spacecraft telemetry limitations often result in CAPS being operated in a mode that alternates brief intervals of relatively high telemetry (e.g., 4 kbits/s) with longer intervals of 500 bits/s. Since during the latter intervals, no TOF data are returned (Table 1), CAPS only provides TOF spectra (usually only 1 or 2 full matrices) during the brief intervals of higher telemetry. Thus, under normal operations, CAPS only returns 1 or 2 TOF spectra as infrequently as once an hour.

Interchange injections seen in Saturn's magnetosphere are typically quite brief (approximately few minutes) [*Chen and Hill*, 2008]. To determine the ion composition of the plasma within such an injection, we would need TOF measurements from an accumulation that was totally enclosed within the event. Given the long accumulation times and low cadence just described, it is difficult to find suitable events under normal operating conditions. However, on occasion, CAPS is allocated a higher spacecraft telemetry rate that enables it to operate continuously in one of the higher instrument rates (see Table 1) that allows the transmission of one 256 s TOF matrix every 256 s for several hours. Interchange injections that occur during such high-data-rate intervals are thus amenable to composition determination by CAPS if they are sufficiently long (>256 s) and if the TOF measurements are made entirely within the event.

We have searched CAPS observations during 2005, 2006, 2007, and 2010 for interchange injection events that may be suitable for determining the composition of the ion population within them. We first used visual inspection of the 6 h energy/time spectrograms available online [http://www.caps.lanl.gov] to identify a large set of interchange injections based on the presence of hotter-than-ambient particles (primarily electrons) and the absence of the cooler ambient particles [see, e.g., *Burch et al.*, 2005]. In the survey range of $r \leq 15\ R_s$, we found 177 events in this initial survey. Of these, 54 matched events identified from Radio and Plasma Wave Science (RPWS) data by *Kennelly et al.* [2013], while 123 did not. For the 101 events that we found at radial distances less than $9\ R_s$ (the outer range of Kennelly events; see Discussion for details), 54 matched Kennelly events, while only 47 did not. It is possible that events that show a clear signature in one data set may be more ambiguous in others, so the roughly 50% of unmatched events may not be surprising. Nonetheless, the fact that more than 50% of our events were also identified by Kennelly et al. is persuasive evidence that both studies were identifying the same sort of event.

Using this set of events, we imposed the further selection criteria for this study: (1) that the event occur during a sustained high-telemetry
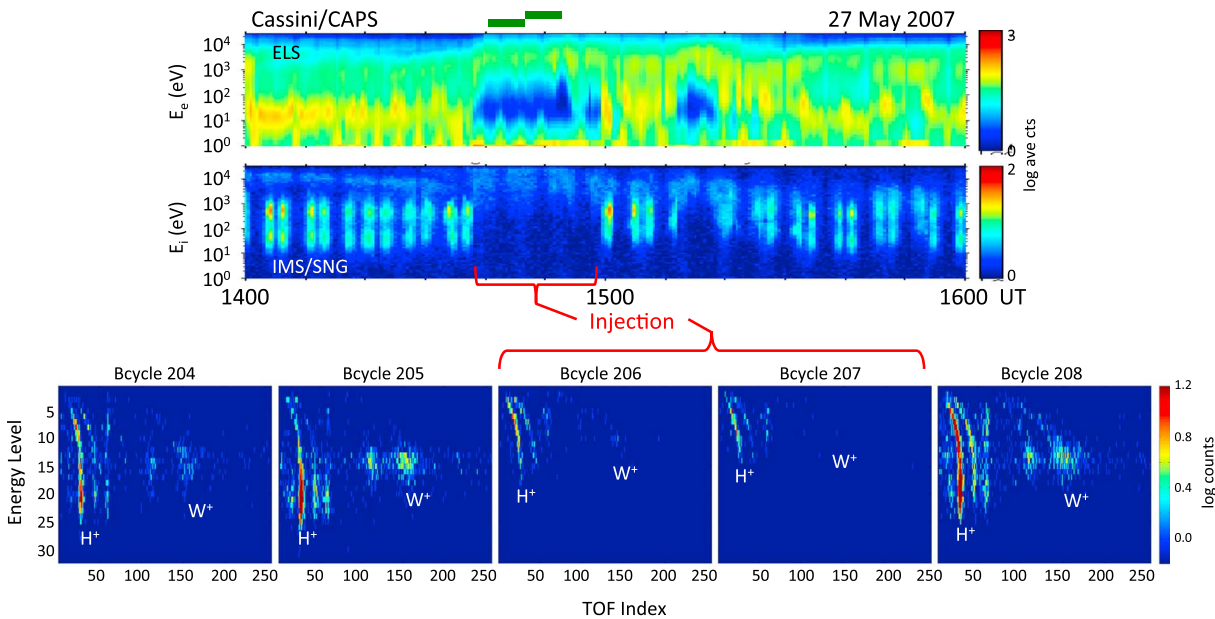
Figure 1. (top) Energy-time spectrograms for ions and electrons observed by CAPS/IMS and ELS for an identified interchange injection event that completely enclosed two full TOF matrix measurements (green bars above the spectrograms). (bottom) A sequence of five consecutive TOF matrices (or Bcycles). The TOF index (abscissa) ranges from 1 to 256 and is related to the measured time of flight as described by *Wilson et al.* [2012]. Bcyles 205 and 206 contain only data from within the hot injection event, while the other Bcycles show the *E/q*-TOF signature of the ambient cooler plasma.

interval (4, 8, or 16 kbits/s), (2) that it be relatively long lasting (>several minutes), and (3) that the event be young in the sense that the hot population shows little evidence of drift dispersion.

We then examined individual 256 s TOF spectra for each event to identify those that captured only the hot injected plasma, unmixed with the cooler plasma adjacent to the injections. We found 13 events that satisfied our criteria (see Table 2). Due to the requirement for relatively long events, our selected set turns out to be limited to rather large L values ($L > 8.2$) because of a correlation between L and interchange event duration that can be found in our original survey of 177 events (not shown). The events at low L are all typically too short to entirely contain a full TOF spectrum. As addressed more extensively in the Discussion section, it is worth noting that previous studies have found that the primary occurrence location of interchange injections is $L\sim4$–11 [e.g., *Chen and Hill*, 2008; *Kennelly et al.*, 2013], but these conclusions may be specific to the selection criteria used in those studies. It is not uncommon to see such events at $L\sim10$–13 and even beyond in CAPS data.

Figure 1 illustrates one of the identified intervals. The upper half of the figure shows count rate spectrograms (count rate is approximately proportional to energy flux) for electrons (from ELS data) and ions (from SNG data) for a 2 h interval on 27 May 2007. The injection event, lasting from ~14:40 to almost 15:00 UT, is characterized by the presence of hot electrons and ions and by the absence of the relatively cool, dense ambient populations that can be seen adjacent to the injection. It is similar to event B on day 183, 2004, described by *Burch et al.* [2005, see their Figure 1] as a "local injection," with little dispersion seen outside the main event.

The five panels in the lower half of Figure 1 show a sequence of individual TOF spectra taken as Cassini traversed the injection. The energy level (ordinate) runs from 1 to 32, with 1 corresponding to the highest energy/charge (~33 keV/e) and 32 corresponding to the lowest energy/charge (~1 eV/e). The TOF index (abscissa) ranges from 1 to 256 and is related to the measured time of flight through a rather complex formula described by *Wilson et al.* [2012]. The color-coded quantity in each plot is the logarithm of the number of counts accumulated in each E/q-TOF bin. The identification of individual species in these TOF matrices is discussed in the Appendix A. Each of the E-TOF panels in the figure has the primary detected species (H^+ and W^+) labeled.

The sequence of TOF spectra in the lower half of Figure 1 shows the clear distinction between the hot, tenuous plasma within the injection event (Bcycles 206 and 207) and the cooler, denser plasma in the ambient medium before and after the event (Bcycles 204, 205, and 208). It is also clear that the two injection spectrograms show only the hot injection plasma with no admixture of the ambient cooler material. One of the striking aspects of the injection plasma, in addition to the higher temperature, is the apparent lack of water-group ions; indeed, there are very few identifiable W^+ counts in either injection spectrum. In the following section, we will quantify this apparent heavy ion depletion. To help with this quantification, we have selected one or two control intervals of ambient plasma in the vicinity of each of the identified injection intervals. The selection criteria for the control events are the opposite of those for the injection events, namely, they are intervals in which the spectra are clearly dominated by the cooler ambient material. These also are listed in Table 2.

3. Analysis

As described in the Appendix A, each of the major species in which we are interested (H^+, H_2^+, and W^+) occupies a known region of TOF at each energy level. To quantify the relative ion composition within the injection events, we sum the counts at each energy level that lie within the TOF ranges identified for each of these species, combining all of the individual TOF spectra that we identify as "pure" injection material (i.e., combining all the spectra that show no admixture of ambient material). We then estimate the "pseudodensity" of each species by the following means:

Because the TOF data represent an integration over all the viewing directions (all eight anodes and all actuation angles) included in the 256 s accumulation interval, they contain no information about the angular distribution of the plasma. Thus, we simply assume that the plasma is approximately isotropic. The directional SNG data show that this is a relatively good assumption for the injection plasma, but for the control intervals, the plasma is more directional, usually exhibiting rather strong dependence on the instrument viewing direction [e.g., *Thomsen et al.*, 2010]. Thus, the assumption of isotropy does not properly weigh the different look sectors, and the absolute derived densities will not be accurate. Nonetheless, even in the more directional cases, the three major species generally have roughly the same dependence on direction so that the relative composition (i.e., the density ratio) is not as sensitive to the viewing as the actual densities themselves.

The number density of a given species j can be calculated by integrating the phase space density f_j over all velocity space:

$$n_j = \int f_j(\mathbf{v})d^3\mathbf{v} \approx \sum_{all\ \Delta\mathbf{v}_i} f_{ij}(E_i)\Delta\mathbf{v}_i \tag{1}$$

where for an isotropic distribution, the element of velocity space $\Delta\mathbf{v}_i$ is the volume of the spherical shell at the speed v_i corresponding to energy E_i:

$$\Delta\mathbf{v} \approx 4\pi v_i^2 dv$$
$$\approx 4\pi\sqrt{\frac{2(E/q)_i}{(m_j/q_j)^3}}\Delta(E/q)_i \tag{2}$$

The phase space density in equation (1) is related to the counts measured in the IMS instrument by the expression

$$f_{ij} \approx \frac{(m_j/q_j)^2}{2(E/q)_i^2\,\varepsilon_{ij}G_i\tau}C_j(E/q)_i \tag{3}$$

where

$$C_j(E/q)_i = \sum_{k=TOF1(i,j)}^{k=TOF2(i,j)} C_{ijk} \tag{4}$$

is the sum of counts observed at the ith energy per charge level within the TOF range identified for that energy for the jth species. In equation (3), τ is the accumulation time for the counts at each energy level (=7 s for a single TOF spectrum), G_i is the energy-dependent geometric factor for all eight anodes of
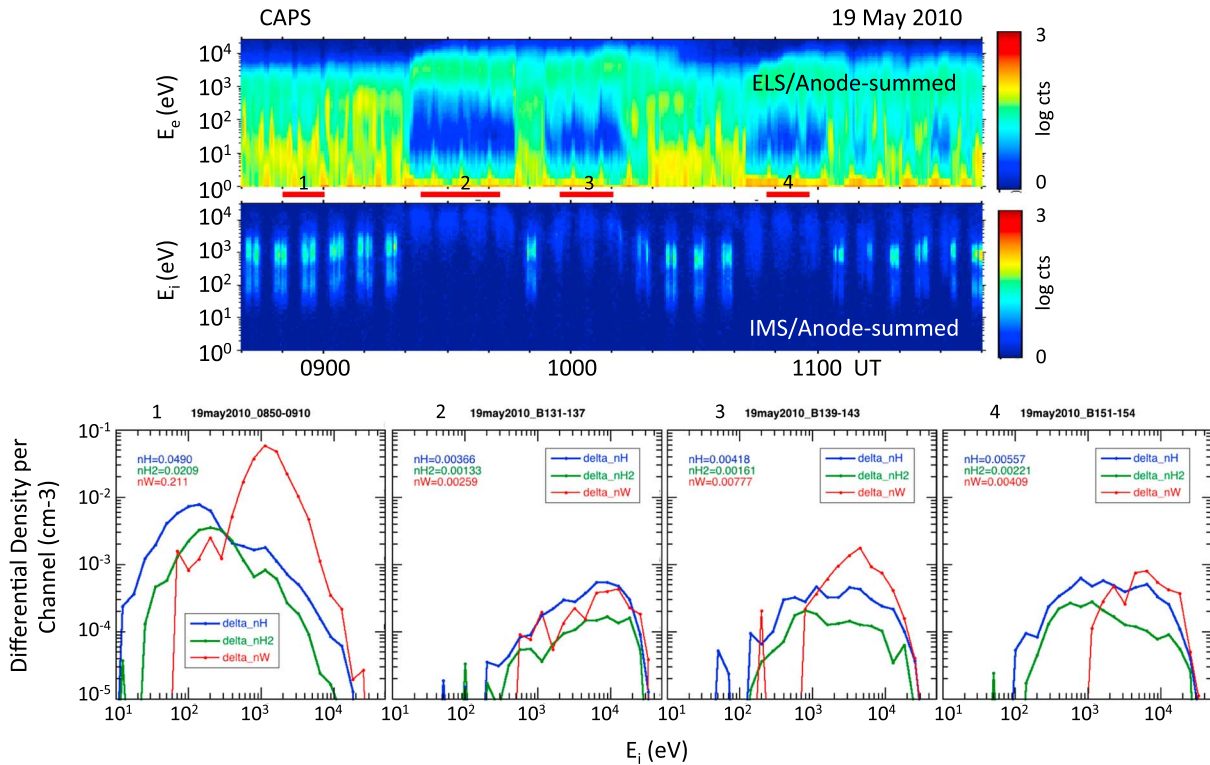
Figure 2. (top) Energy-time spectrograms for ions and electrons observed by CAPS/IMS and ELS for three identified interchange injection events on 19 May 2010. (bottom) Differential contributions to the density of each species within each CAPS energy channel for the four intervals indicated with red bars between the two spectrograms. Interval 1 is a control interval of ambient plasma measurements, and intervals 2–4 were all entirely within the three injection events. Within each of the differential density plots, the total energy-integrated densities for the three major species are given.

the electrostatic analyzer (Table A2) [c.f., *Wilson et al.*, 2012], and ε_{ij} is the energy- and species-dependent efficiency for detection in the TOF section (see Appendix A). Equation (1) then becomes

$$n_j \approx \frac{4\pi}{\tau} \sqrt{\frac{(m_j/q_j)}{2}} \sum_i \frac{C_j(E/q)_i \Delta(E/q)_i}{G_i \varepsilon_{ij}(E/q)_i^{3/2}} \tag{5}$$

Figure 2 illustrates the outcome of this calculation for the three injection events and one control interval on 19 May 2010. The upper half of the figure shows the energy-time spectrograms for ions and electrons for the 3 h interval from 08:40 to 11:40 UT. The red bars below the spectrograms indicate the three events and one control interval analyzed on this day. The lower half of the figure shows the resulting differential density profiles for the three major species for each of the intervals, calculated according to equation (5), but prior to the summation over E/q. Thus, the quantities plotted are the differential contribution to the total density from each of the CAPS energy channels. The inserts in each panel give the full integrated densities of each species (i.e., summed over energy as indicated in equation (5)). The first panel in the set corresponds to the control interval. It is immediately obvious that the densities in the injection events are substantially (by a factor of 10 or more) lower than those in the control interval. Moreover, as already anticipated from the spectrogram in the upper half of the figure, the spectral shape in the events is radically different from the control, being clearly hotter for all three species than in the local ambient population. The other important point about the differential densities is that they are clearly declining to small values by the highest energies, indicating that the bulk of the density of this population lies well within the CAPS energy range.

Figure 3 is similar to Figure 2 but for the injection event on 2 June 2010. The characteristics are very similar to those described above but with a slight hint of the presence of a lower-energy component to the light ions of much lower intensity than in the ambient population.
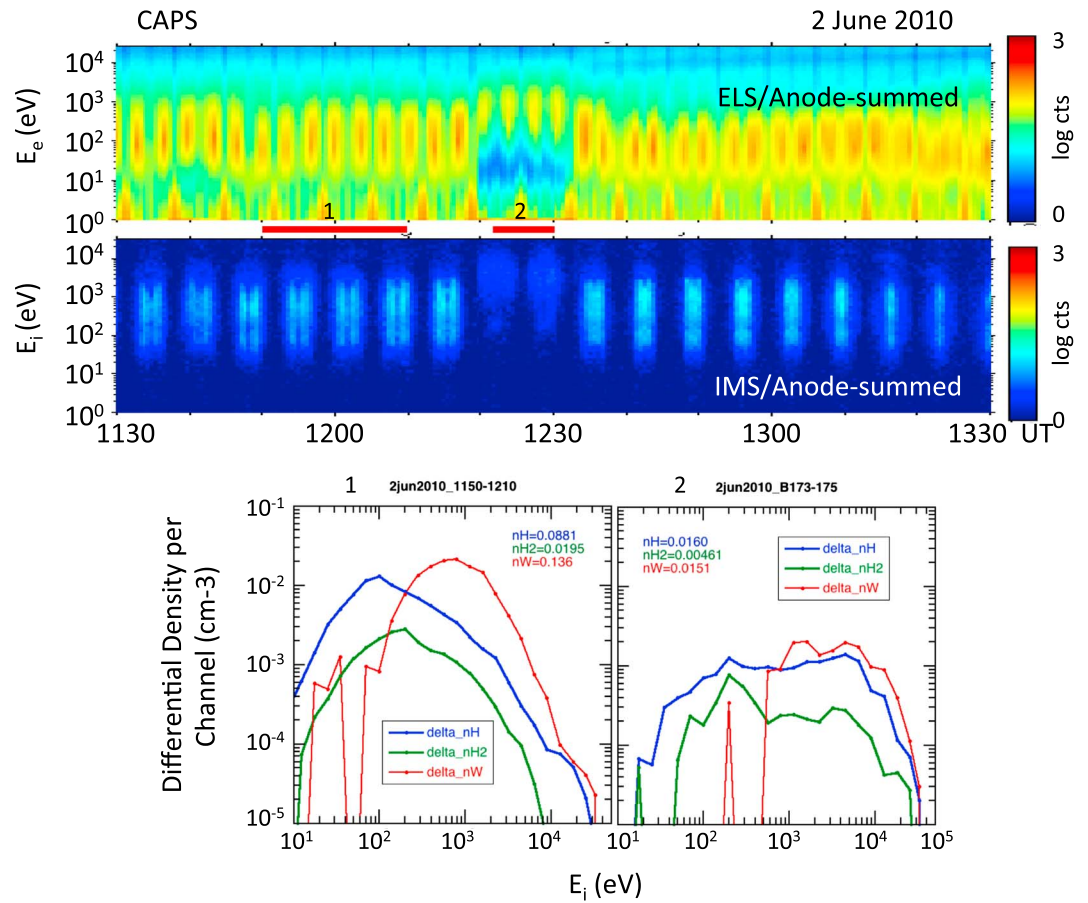
Figure 3. Similar to Figure 2 but for an injection event on 2 June 2010.

4. Results and Discussion

Figure 4 shows the results of this calculation for all 13 of the identified events, with the derived density ratios for H_2^+/H^+ and W^+/H^+ plotted as a function of the dipole L shell of the observation. Each of the events (squares) is connected by a solid line to its corresponding control interval (dots). Figure 4a indicates
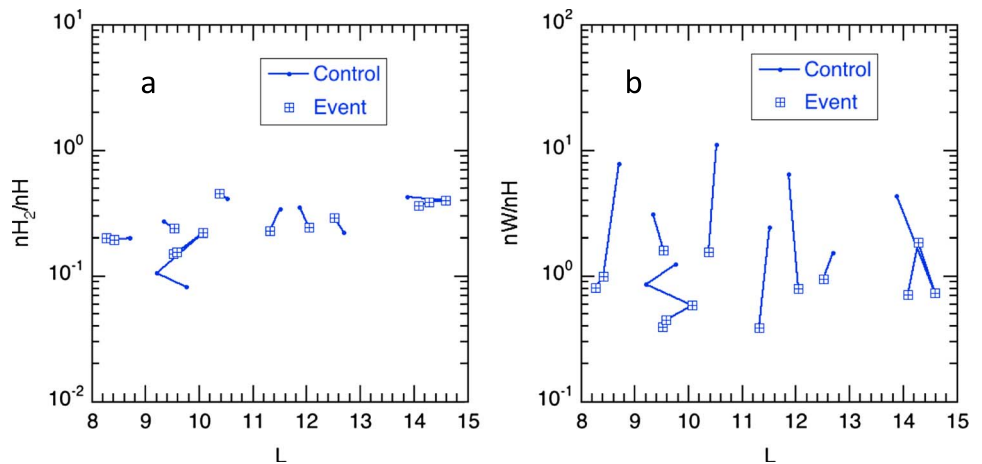

Figure 4. Comparison of the derived density ratios from within the 13 injection events (squares) with the density ratios from the control intervals (dots connected to the corresponding squares with solid lines). The density ratios for (a) H_2^+/H^+ and (b) W^+/H^+ are shown as a function of dipole L value.
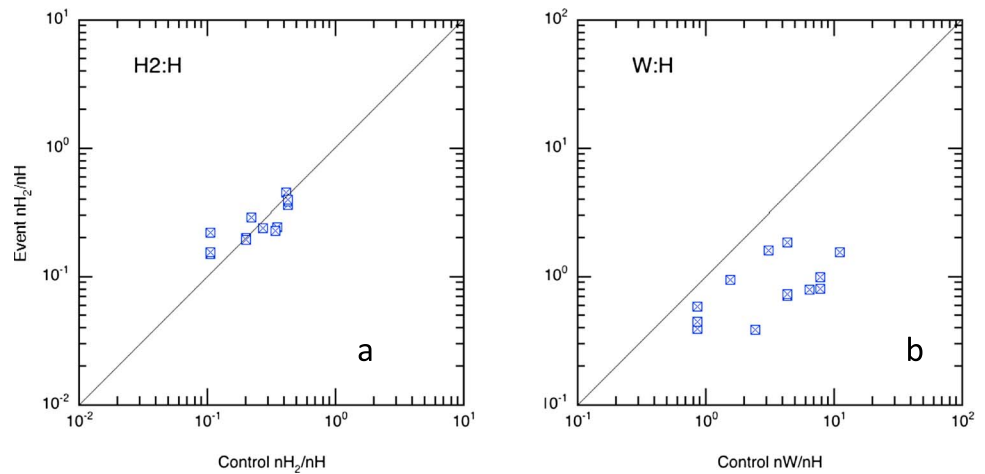
Figure 5. Density ratios within the injection events plotted as a function of the density ratios in the corresponding control intervals for (a) H_2^+/H^+ and (b) W^+/H^+.

that the light-ion density ratios within the events are quite similar to those in the adjacent control intervals. Figure 4b, on the other hand, shows a clear reduction in W^+/H^+ in the events compared to the control intervals. This depletion ranges from a factor of nearly 2 to almost an order of magnitude. Figure 5 shows the density ratio in the events plotted as a function of the density ratio in the corresponding control intervals, emphasizing the same finding that the water-group ions show a significant depletion relative to H^+ in the injected plasma compared to the ambient, with little change seen in the light-ion ratio.

The water-group depletion in the injection plasma confirms that such intervals are not the result of local heating of the plasma but correspond to the arrival of new plasma from some other source location. To help establish the source location, we examine in Figure 6 the radial variation of the density ratios observed in the full CAPS data set of numerical moments, constrained to low latitudes (within 10° of the equatorial plane) and to intervals where CAPS was viewing the corotation direction (see, e.g., *Thomsen et al.* [2010]). In Figure 6, we show the occurrence distribution of the observed density ratios for each $2\,R_s$ interval from $L = 6$ to 20. The 1, 25, 50, 75, and 99 percentile levels are indicated.

The variation of H_2^+/H^+ over this radial range is rather slight (Figure 6a), with an increase toward the middle/outer magnetosphere, which we have previously attributed to the addition of light ions from Titan's
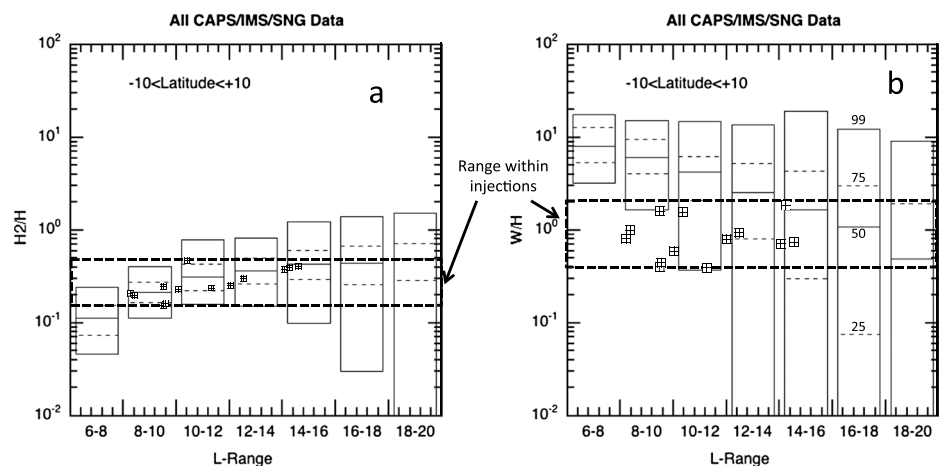

Figure 6. Occurrence distribution of density ratios determined from standard production moments [*Thomsen et al.*, 2010] for low-latitude measurements (within 10° of the equatorial plane) in $2\,R_s$ bins between dipole L values of 8 and 20. The 1, 25, 50, 75, and 99 percentile levels are shown for (a) H_2^+/H^+ and (b) W^+/H^+. The square symbols are the density ratios measured within the 13 injection events, and the dashed boxes enclose the range of those injection ratios.

neutral torus [*Thomsen et al.*, 2010]. In principle, the species identified as H_2^+ could also be He^{++}, a solar wind marker ion. However, this ratio can approach 1 in the outer magnetosphere, well above the typical value of a few percent in the solar wind, indicating that the plasma of the outer magnetosphere is largely of internal rather than solar wind origin [*Thomsen et al.*, 2010]. By contrast, the water-group ratio W^+/H^+ declines rather steeply with L either as a consequence of the addition of Titan-derived light ions in the outer magnetosphere or as a consequence of preferential loss of heavy ions in the shedding of plasma in tail reconnection events as discussed in previous work [e.g., *Badman and Cowley*, 2007; *Thomsen et al.*, 2013].

Superimposed on these occurrence distributions for the full CAPS data set in Figure 6 are the measured density ratios from within the injection events plus dashed boxes indicating the range of these density ratios. The light-ion ratios in the injections are consistent with the observed ratio over a wide range of L, but it is clear that one needs to look to L greater than about 14 to find typical W^+/H^+ ratios that are as low as those observed within the injection events. Thus, the observed injections may have traveled as much as 6 R_s before they were observed by Cassini.

As noted above, Table 2 reveals that the events in our data set typically occurred at rather large radial distances, all beyond ~8.2 R_s and extending out as far as 14.6 R_s. This may seem surprising in light of the findings of *Hill et al.* [2005] and *Chen and Hill* [2008] that 95% of the interchange injections identified occurred at $r < 10\ R_s$. Similarly, *Kennelly et al.* [2013], in a survey of young events observed in RPWS data, found no events beyond 11 R_s and noted the similarity of the radial distribution they found to that identified by Chen and Hill. The fact that our events are at and beyond the outer distance determined from these earlier studies is due to several issues having to do with event identification:

First, *Kennelly et al.* [2013] identified events primarily based on a lowering of the local upper hybrid frequency in the RPWS data. Thus, one of their requirements was the presence of a strong background upper hybrid emission. It turns out that beyond r~9–10 R_s, the upper hybrid emissions become quite weak, making it difficult to identify and thus placing an upper limit on the range over which interchange injections can be identified on that basis. As noted above, a comparison of our original set of events identified with CAPS data alone matched 50% with Kennelly events inside of 9 R_s, but had zero matches at larger distances, where Kennelly et al. identified essentially no events.

Second, *Hill et al.* [2005] and *Chen and Hill* [2008] focused on "older" events, with clear dispersive signatures in both ions and electrons, because they were interested in estimating the ages. Because of the common presence of higher-energy particles in the outer magnetosphere ($r \geq 10$), it is difficult to identify clean dispersive signatures there, perhaps accounting for the paucity of interchange injections at larger radial distances in those studies. In *Chen et al.* [2010], the requirement of clean dispersive signatures was relaxed, but the study only addressed events between $r = 5$ and $r = 10$.

Thus, it seems likely that the radial distribution of identified interchange events depends significantly on the identification criteria. Our search based on the CAPS spectral signature reveals a significant number of events beyond 9 R_s, confirming the finding from our composition results that such events extend well into the middle magnetosphere (see also the simulation results of *Liu et al.* [2010], who find interchange "fingers" extending at least out to 12 R_s and probably beyond).

5. Summary

We have identified 13 interchange injection events that were sufficiently long in duration and during which CAPS was in a high telemetry rate mode such that TOF spectra could be obtained from entirely within the events. Using the TOF data to separate the main ion species H^+, H_2^+, and W^+, we calculated approximate densities of each species under the assumption that all distributions were isotropic. These estimated densities are likely to be wrong if the distributions are not isotropic, but if the angular distributions of the various species are not greatly different from each other, the ratio of the estimated densities should be rather insensitive to the departures from isotropy. We find that the light-ion density ratio, H_2^+/H^+, in the injection events is not discernibly different from that ratio in control intervals from the ambient plasma. Typical values of the ratio in both the injection events and the ambient plasma are in the range of 0.1–0.4, well above the value of a few percent expected for plasma of solar wind origin.
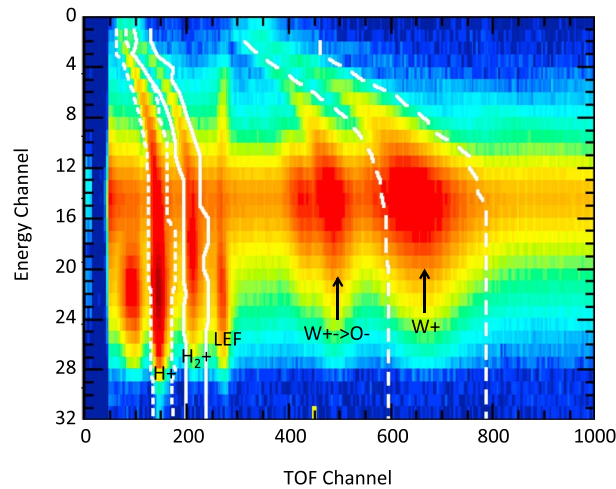
Figure A1. E/q versus TOF matrix compiled from TOF measurements obtained in the intervals listed in Table A1. The ordinate is the energy channel number (see Table A2), and the abscissa is the TOF channel number. Individual ion species occupy unique regions in E/q-TOF space as indicated by the labels. White lines show the adopted TOF ranges determined as described in the text.

By contrast, the water-group ratio, W^+/H^+, shows significantly lower values than ambient. We have compared the measured density ratios with the range of values observed throughout Saturn's magnetosphere (based on our production moments [*Thomsen et al.*, 2010]). In the full data set, H_2^+/H^+ varies little throughout the region from $L\sim8$–20, whereas W^+/H^+ declines rather strongly with L. Typical values of W^+/H^+ that are as low as those observed within the injection events are found beyond $L\sim14$, indicating that the injection events are delivering plasma from the outer magnetosphere, at times traveling at least 6 R_s.

Appendix A: Ion Species Determination

The CAPS ion mass spectrometer combines an electrostatic analyzer front end, which allows determination of an entering particle's energy per charge (E/q), with a time-of-flight section, which allows determination of that particle's speed [*Young et al.*, 2004]. There are two TOF detectors: one that detects particles that emerge from the start foil as ions and are reflected by the linear electric field (the so-called LEF detector) and one that detects particles that emerge as neutrals from the start foil, traveling straight through the time-of-flight section to the ST ("straight through") detector. It is the latter (ST) particles that we use in the present study.

The combination of energy per charge and speed yields the particle's mass per charge. For a given species, say H^+, the time of flight is thus uniquely a function of its E/q. Therefore, in a matrix of E/q versus TOF, particles of each species will occupy distinct regions, although with some spread due to scattering and some energy loss in the instrument [e.g., *Young et al.*, 2004; the Appendix A in *Thomsen et al.*, 2010]. Figure A1 shows such a matrix compiled from a large number of TOF data obtained by CAPS at Saturn. The dates and time intervals included in this figure are listed in Table A1.

The ordinate in Figure A1 is the energy channel number for the TOF/ST data product. E/q varies logarithmically from ~1 eV at channel 32 to ~33 keV at channel 1. Likewise, the abscissa is the TOF channel number, which is linearly proportional to the actual time of flight. For a further discussion of the relationship of energy per charge and TOF to these channel numbers, see *Wilson et al.* [2012]. The color in Figure A1 is proportional to the logarithm of the total counts, with red indicating the highest counts and blue the lowest counts accumulated over the sum of the intervals listed in Table A1.

In Figure A1, the regions of E/q-TOF space occupied by the primary species (H^+, H_2^+, and W^+, where $W^+ = O^+$, OH^+, H_2O^+, H_3O^+) are indicated by the corresponding labels. The grouping labeled "LEF" corresponds to counts from secondary electrons produced when an ion strikes the high-resolution LEF section of the TOF chamber [see, e.g., *Young et al.*, 2004]. The grouping labeled "$W^+ \rightarrow O^-$" corresponds to oxygen ions that leave the foil with a negative charge and are accelerated

Table A1. Intervals for Compiling Figure A1

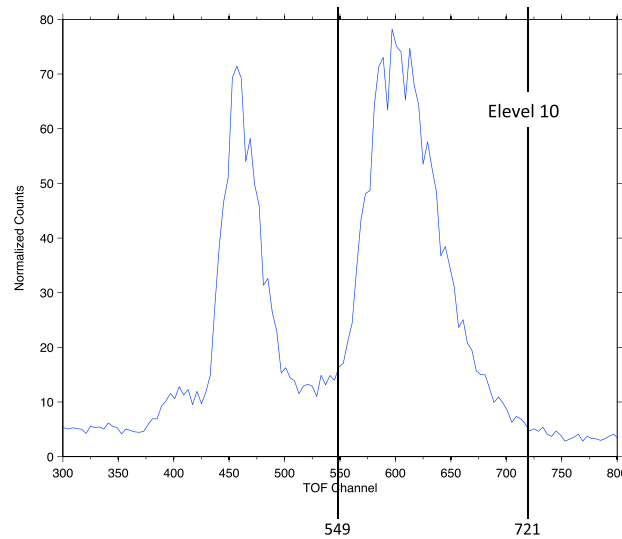| Date (DD-MM-YYYY)	Hour Range
28-10-2004	0–24
21-3-2006	0–24
27-4-2006	0–24
28-4-2006	0–6
16-10-2010	0–12
18-10-2010	0–24
19-10-2010	0–24
29-11-2010	0–24

Figure A2. Slice through the *E/q* versus TOF matrix shown in Figure A1 taken at energy level 10 (2241 eV). This range of TOF encompasses the (right) W^+ peak and the peak for (left) $W^+ \to > O^-$. The adopted TOF channel range for W^+ is shown by the vertical lines.

by the linear electric field in the TOF section arriving with a shorter time of flight than the corresponding neutrals.

The white lines in Figure A1 delineate the regions in *E/q*-TOF space assigned to the various species. To obtain these lines, we have taken 1-D cuts through the matrix plotted in Figure A1 at each of the 32 energy levels. Such a cut for energy level 10 (2241 eV) is shown in Figure A2. The lower and upper TOF channels that enclose the full peak (W^+, for the case in Figure A2) were identified from such cuts at each energy level, supplemented with additional information from numerical modeling of the instrument response [e.g., see Appendix A of *Thomsen et al.*, 2010]. The adopted TOF channels that bracket each species at each of the 32 energy levels are listed in Table A2. Note that the energies listed for the various channels

Table A2. TOF Limits and Efficiencies (IMS Sweep Table 2)

Energy Level	Energy (eV)	G (cm² sr eV/eV)	H Start Chan	H Stop Chan	H Eff	H2 Start Chan	H2 Stop Chan	H2 eff	W Start Chan	W Stop Chan	W Eff
1	32,771	0.00531	61	81	0.0151	97	129	0.0506	313	461	0.0270
2	32,771	0.00531	61	81	0.0151	101	129	0.0506	313	461	0.0270
3	25,362	0.00535	63	93	0.0169	93	141	0.0543	341	461	0.0263
4	17,938	0.00540	77	113	0.0199	113	173	0.0599	377	509	0.0255
5	12,681	0.00546	85	129	0.0239	129	169	0.0665	413	545	0.0248
6	8,968.8	0.00552	93	137	0.0289	145	185	0.0745	449	601	0.0240
7	6,343.3	0.00558	101	145	0.0349	157	193	0.0838	481	631	0.0232
8	4,481.6	0.00564	109	145	0.0413	165	201	0.0934	513	665	0.0225
9	3,168.8	0.00571	113	153	0.0472	173	209	0.1022	533	681	0.0218
10	2,240.8	0.00578	117	161	0.0520	177	217	0.1093	549	721	0.0213
11	1,584.4	0.00586	121	161	0.0556	177	225	0.1136	561	753	0.0207
12	1,120.8	0.00593	121	161	0.0580	185	225	0.1161	569	753	0.0203
13	792.68	0.00602	125	161	0.0592	193	225	0.1170	577	769	0.0200
14	560.42	0.00610	125	161	0.0596	193	225	0.1170	581	769	0.0198
15	396.27	0.00619	125	161	0.0597	193	225	0.1170	585	785	0.0196
16	280.29	0.00628	125	161	0.0601	193	241	0.1175	589	785	0.0196
17	198.21	0.00638	125	177	0.0612	193	241	0.1196	589	785	0.0198
18	140.07	0.00649	125	177	0.0630	193	241	0.1232	589	785	0.0200
19	99.030	0.00659	125	177	0.0657	193	233	0.1277	589	785	0.0203
20	70.030	0.00671	125	177	0.0690	193	233	0.1327	593	785	0.0207
21	49.510	0.00683	125	177	0.0722	193	241	0.1377	593	785	0.0211
22	35.030	0.00695	129	169	0.0745	197	241	0.1405	593	785	0.0212
23	24.770	0.00708	129	169	0.0754	193	241	0.1399	593	785	0.0211
24	17.510	0.00722	129	169	0.0750	193	241	0.1374	593	785	0.0207
25	12.390	0.00737	129	169	0.0742	193	237	0.1344	593	785	0.0204
26	8.7600	0.00752	129	169	0.0737	197	237	0.1330	593	785	0.0202
27	6.1900	0.00768	129	169	0.0736	197	237	0.1330	593	785	0.0202
28	4.3800	0.00784	129	177	0.0736	197	237	0.1330	593	785	0.0202
29	3.0900	0.00802	133	169	0.0736	197	237	0.1330	593	785	0.0202
30	2.1900	0.00820	133	169	0.0736	197	237	0.1330	593	785	0.0202
31	1.5500	0.00839	133	173	0.0736	197	237	0.1330	593	785	0.0202
32	1.1900	0.00855	133	173	0.0736	197	237	0.1330	593	785	0.0202

in Table A2 are for IMS Sweep Table 2 [c.f., *Wilson et al.*, 2012]. All of the events in this study were obtained with Sweep Table 2 except those on 27 May 2007, which were obtained using Sweep Table 1. Tables 1 and 2 are identical except for the highest two channels. In the analysis used here, the top channel is ignored, and the contribution to the density from the second channel will be underestimated by 30% if Table 2 energies are used during Table 1 intervals.

In addition to the range of TOF channels to attribute to each species, the calculation leading to equation (5) requires knowledge of the detection efficiency ε_{ij} for species j at energy per charge $(E/q)_i$. The efficiencies for the full time-of-flight detection of each species have been determined using an ion-optics simulation (SIMION) of the top hat and LEF sections of IMS in combination with laboratory data on the exit charge state partitioning of ions passing through carbon foils, secondary electron emission yields from the foils, and microchannel plate detection efficiencies for ions and electrons. We expect the systematic uncertainty in these efficiencies to be on the order of ±20% at the one sigma level. The resulting efficiencies are listed in Table A2. At each energy, these efficiencies relate the total counts that lie between the TOF limits given in the table to the total incident flux of a given species (e.g., equation (3)).

References

André, N., M. K. Dougherty, C. T. Russell, J. S. Leisner, and K. K. Khurana (2005), Dynamics of Saturnian inner magnetosphere: First inferences from the Cassini magnetometers about smallscale plasma transport in the magnetosphere, *Geophys. Res. Lett.*, *32*, L14S06, doi:10.1029/2005GL022643.

André, N., et al. (2007), Magnetic signatures of plasma-depleted flux tubes in the Saturnian inner magnetosphere, *Geophys. Res. Lett.*, *34*, L14108, doi:10.1029/2007GL030374.

Badman, S. V., and S. W. H. Cowley (2007), Significance of Dungey-cycle flows in Jupiter's and Saturn's magnetospheres, and their identification on closed equatorial field lines, *Ann. Geophys.*, *25*, 941.

Burch, J. L., J. Goldstein, T. W. Hill, D. T. Young, F. J. Crary, A. J. Coates, N. André, W. S. Kurth, and E. C. Sittler Jr. (2005), Properties of local plasma injections in Saturn's magnetosphere, *Geophys. Res. Lett.*, *32*, L14S02, doi:10.1029/2005GL022611.

Chen, Y., and T. W. Hill (2008), Statistical analysis of injection/dispersion events in Saturn's inner magnetosphere, *J. Geophys. Res.*, *113*, A07215, doi:10.1029/2008JA013166.

Chen, Y., T. W. Hill, A. M. Rymer, and R. J. Wilson (2010), Rate of radial transport of plasma in Saturn's inner magnetosphere, *J. Geophys. Res.*, *115*, A10211, doi:10.1029/2010JA015412.

Hill, T. W., A. M. Rymer, J. L. Burch, F. J. Crary, D. T. Young, M. F. Thomsen, D. Delapp, N. André, A. J. Coates, and G. R. Lewis (2005), Evidence for rotationally driven plasma transport in Saturn's magnetosphere, *Geophys. Res. Lett.*, *32*, L14S10, doi:10.1029/2005GL022620.

Kennelly, T. J., J. S. Leisner, G. B. Hospodarsky, and D. A. Gurnett (2013), Ordering of injection events within Saturnian SLS longitude and local time, *J. Geophys. Res. Space Physics*, *118*, 832–838, doi:10.1002/jgra.50152.

Kidder, A., R. M. Winglee, and E. M. Harnett (2009), Regulation of the centrifugal interchange cycle in Saturn's inner magnetosphere, *J. Geophys. Res.*, *114*, A02205, doi:10.1029/2008JA013100.

Liu, X., and T. W. Hill (2012), Effects of finite plasma pressure on centrifugally driven convection in Saturn's inner magnetosphere, *J. Geophys. Res.*, *117*, A07216, doi:10.1029/2012JA017827.

Liu, X., T. W. Hill, R. A. Wolf, S. Sazykin, R. W. Spiro, and H. Wu (2010), Numerical simulation of plasma transport in Saturn's inner magnetosphere using the Rice Convection Model, *J. Geophys. Res.*, *115*, A12254, doi:10.1029/2010JA015859.

Mauk, B. H., et al. (2005), Energetic particle injections in Saturn's magnetosphere, *Geophys. Res. Lett.*, *32*, L14S05, doi:10.1029/2005GL022485.

Rymer, A. M., B. H. Mauk, T. W. Hill, C. Paranicas, D. G. Mitchell, A. J. Coates, and D. T. Young (2008), Electron circulation in Saturn's magnetosphere, *J. Geophys. Res.*, *113*, A01201, doi:10.1029/2007JA012589.

Rymer, A. M., et al. (2009), Cassini evidence for rapid interchange transport at Saturn, *Plan. Space Sci.*, *57*, 1779–1784.

Thomsen, M. F. (2013), Saturn's magnetospheric dynamics, *Geophys. Res. Lett.*, *40*, 5337–5344, doi:10.1002/2013GL057967.

Thomsen, M. F., D. B. Reisenfeld, D. M. Delapp, R. L. Tokar, D. T. Young, F. J. Crary, E. C. Sittler, M. A. McGraw, and J. D. Williams (2010), Survey of ion plasma parameters in Saturn's magnetosphere, *J. Geophys. Res.*, *115*, A10220, doi:10.1029/2010JA015267.

Thomsen, M. F., R. J. Wilson, R. L. Tokar, D. B. Reisenfeld, and C. M. Jackman (2013), Cassini/CAPS observations of duskside tail dynamics at Saturn, *J. Geophys. Res. Space Physics*, *118*, 5767–5781, doi:10.1002/jgra.50552.

Wilson, R. J., R. L. Tokar, M. G. Henderson, T. W. Hill, M. F. Thomsen, and D. H. Pontius Jr. (2008), Cassini plasma spectrometer thermal ion measurements in Saturn's inner magnetosphere, *J. Geophys. Res.*, *113*, A12218, doi:10.1029/2008JA013486.

Wilson, R. J., F. Crary, L. K. Gilbert, D. B. Reisenfeld, J. T. Steinberg, and R. Livi (2012), Cassini Plasma Spectrometer (CAPS) PDS User's Guide, available electronically at http://ppi.pds.nasa.gov/search/view/?f=yes&id=pds://PPI/CO-E_J_S_SW-CAPS-2-UNCALIBRATED-V1.0/DOCUMENT/CAPS_USER_GUIDE/CAPS_PDS_USER_GUIDE_V1_00&o=1.

Young, D. T., et al. (2004), Cassini Plasma Spectrometer investigation, *Space Sci. Rev.*, *114*, 1–112.